


## Article

# Experimental Study on Streamwise Vortex-Induced Vibration of a Flexible, Slender Cylinder

Wanhai Xu <sup>1,2</sup> , Wenqi Qin <sup>1</sup> and Xifeng Gao <sup>1,\*</sup>

<sup>1</sup> State Key Laboratory of Hydraulic Engineering Simulation and Safety, Tianjin University, Tianjin 300072, China; xuwanhai@tju.edu.cn (W.H.X.); qinwenqi@tju.edu.cn (W.Q.Q.)

<sup>2</sup> Collaborative Innovation Centre for Advanced Ship and Deep-Sea Exploration, Shanghai 200240, China

\* Correspondence: gaoxifeng@tju.edu.cn

Received: 31 January 2018; Accepted: 16 February 2018; Published: 22 February 2018

**Abstract:** Laboratory tests on streamwise vortex-induced vibration (VIV) of a flexible, slender cylinder were carried out in a towing tank. A cylinder model, 20 mm in diameter and 3.91 m in length, was towed horizontally to generate a uniform profile of relative velocity in calm water. The aspect ratio (length to diameter) and mass ratio (structural mass to displaced fluid mass) of the cylinder were 195.5 and 1.39, respectively. The Reynolds number was in the range of 1000–3000. The displacement amplitudes and vibration frequencies were investigated in order to examine the dynamic characteristics of the flexible cylinder undergoing streamwise VIV. Experimental results indicated that there were two detached branches in the streamwise response curve, i.e., the first excitation region ( $1.0 < Vr < 2.6$ ) and the second excitation region ( $2.6 < Vr < 4.0$ ). This phenomenon is similar to the streamwise VIV of an elastically-mounted rigid cylinder, except that a larger and shifted peak was observed in the second branch in this study. The cylinder's linear orbits in the first excitation region indicated that the streamwise vibration frequency was equivalent to its transverse counterpart. However, in the second excitation region, the cylinder's motion showed a figure-of-eight pattern, and the streamwise frequency was twice that in the transverse direction. In addition, two curve-fitted formulae of the maximum displacement amplitudes in the first and second excitation regions, versus the reduced mass-damping parameter, were proposed. This was accomplished by compiling the published streamwise VIV data and those in the present research work.

**Keywords:** vortex-induced vibration; excitation region; streamwise; flexible cylinder

## 1. Introduction

Vortex-induced vibration (VIV) of a flexible, slender cylinder is a complicated fluid–structure interaction (FSI) phenomenon that may result in structural failure, due to fatigue damage accumulation. It is a problem of both industrial and academic interest, and has been studied for decades. Several key reviews and important milestones on this topic can be found in Naudascher [1], Norberg [2], Sarpkaya [3], Gabbai and Benaroya [4], Williamson and Govardhan [5], Wu et al. [6], Cagney and Balabani [7], and Feng et al. [8].

The vast majority of previous work has focused on 2-degree-of-freedom (2-DOF) VIV of a cylinder in both transverse and streamwise directions [9–11], and on 1-degree-of-freedom (1-DOF) VIV in the transverse direction [12–14]. A generally accepted understanding is that the response amplitude and the fluctuating fluid force in the streamwise direction are one order of magnitude smaller than those in the transverse direction [15], and the streamwise vibrations are trivial and can be neglected in fatigue analysis. However, the recent experiments of Baarholm et al. [16] on VIV of a flexible, slender cylinder showed that the streamwise responses might have a significant contribution to fatigue under tension-controlled conditions. This is because the streamwise vibrations take place at double

the frequency and half the wavelength of those in the transverse direction. Given that the curvature is inversely proportional to the squared wavelength, fatigue caused by the streamwise vibrations dominates when the flow velocity is low.

Due to its importance and less well-established dynamic behaviors, the streamwise VIV of an elastically supported, rigid, circular cylinder has been extensively studied. These investigations are ongoing. The pioneer work can be backtracked to Aguirre [17], in which the response regimes of streamwise VIV were characterized. Currie and Turnbull [18] introduced a wake-oscillator model for predicting the VIV of a cylinder in the streamwise direction. Sumer and Fredsøe [19] concluded from 2-DOF VIV experiments that there were three types of streamwise VIV. The first type originated from the symmetric vortex shedding in  $1.0 < Vr < 2.3$  ( $Vr = u / f_1 D$ , where  $Vr$  is the reduced velocity,  $u$  is the flow velocity,  $f_1$  is the natural frequency of the vibration system, and  $D$  is the cylinder diameter). The second type was caused by the alternate vortex shedding in  $2.3 < Vr < 3.8$ . The third type occurred concurrently with the transverse vibrations in a higher region of  $Vr$ . Okajima et al. [20] performed laboratory tests on the streamwise VIV of a circular cylinder, either spring-mounted at both ends (two-dimensional (2D)), or cantilevered on one end (three-dimensional (3D)) in a water tunnel at subcritical Reynolds numbers. It was found that, in the 2D cases, the response amplitudes were sensitive to the reduced mass-damping parameter  $C_n$  ( $C_n = 2m^*\zeta$ , where  $m^*$  is the mass ratio, and  $\zeta$  is the structural damping ratio) in the first excitation region with symmetrically-shed vortices. While a “lock-in”, similar to that in the transverse VIV, occurred in the second excitation region with alternately-shed vortices. Nishihara et al. [21] experimentally investigated the forced vibration of a circular cylinder in the streamwise direction. It was found that the added mass coefficient, which significantly affects the dynamic behaviors of low mass-ratio VIV, varied greatly in the two excitation regions, while the added damping coefficient could be negative. Cagney and Balabani [22] investigated the near-wake modes of a 1-DOF cylinder undergoing streamwise VIV by using the particle-image velocimetry (PIV). Two modes—the S-I mode (in which two symmetric vortices are shed simultaneously per vibration cycle) and the A-II mode (similar to the well known von Kármán vortex street)—were observed in the first excitation region. One mode, i.e., the SA mode (treated as a special case of the A-II mode), was found in the second excitation region. The competition between the S-I and A-II modes in the first excitation region and transient behaviors of the wake were further analyzed in Cagney and Balabani [23]. It was found that the first excitation region was actually dominated by the A-II mode, characterized by alternate vortex shedding, which contradicted the common assumption that the vortex shedding was symmetric in the entire first excitation region. Later work by the same researchers investigated the streamwise VIV of a 2-DOF pivoted cylinder. It was found that the 2-DOF response regimes were similar to the previous 1-DOF results, and the additional degree of freedom did not significantly alter the vortex-shedding process [7].

Investigation on the streamwise VIV of a rigid, circular cylinder has proliferated in recent years. By contrast, only a few researchers have investigated the streamwise VIV dynamic mechanism of flexible, slender cylinders. King et al. [24] experimentally investigated the streamwise VIV of a cantilevered flexible cylinder with an aspect ratio of 41 in a water channel facility. It was found that large amplitude vibration could be excited at low reduced velocities when  $C_n$  was smaller than 1.0. Few researchers have focused on the prediction of streamwise-only VIV of flexible cylinders, such as marine riser and submarine free spanning pipeline. Several prediction models were proposed to analyze the features of streamwise response undergoing vortex shedding [25–28]. Until now, experimental studies on the streamwise VIV of a flexible circular cylinder, especially with a large aspect ratio and a low mass ratio, were lacking. A series of laboratory experiments were conducted in a towing tank facility to investigate the streamwise VIV of a flexible slender cylinder with a large aspect ratio and a low mass ratio. The statistical characteristics and instantaneous dynamic behaviors of the cylinder model undergoing streamwise VIV were presented and discussed.

The organization of the rest of this paper is as follows: Section 2 presents a description of the experimental set-up; in Section 3, a modal analysis method for the measurement data is introduced;

experimental results and discussions are presented in Section 4; finally, some conclusions are drawn in Section 5.

## 2. Experimental Set-Up

It is well known that there are three types of streamwise VIV, namely, the types falling in the first, second, and third instability region. The first excitation region originates from symmetric vortex shedding in the lower reduced velocity region of  $1.0 < Vr < 2.3$ , and the second excitation region from alternate vortex shedding in the higher reduced velocity region of  $2.3 < Vr < 3.8$  [19]. The first and second instability regions constitute the pure streamwise regime, which is the main focus of our present research work. The third streamwise VIV region of slender marine structures occurs for reduced velocities where transverse oscillations have started. Our experiment was performed in the towing tank at the State Key Laboratory of Hydraulic Engineering Simulation and Safety of Tianjin University. The towing tank is 137.0 m long, 7.0 m wide and 3.3 m deep. A test apparatus, which had a supporting frame, two vertical supporting mechanisms, a cylinder model, and an axial tension system, was designed. The schematic model of the apparatus is shown in Figure 1.

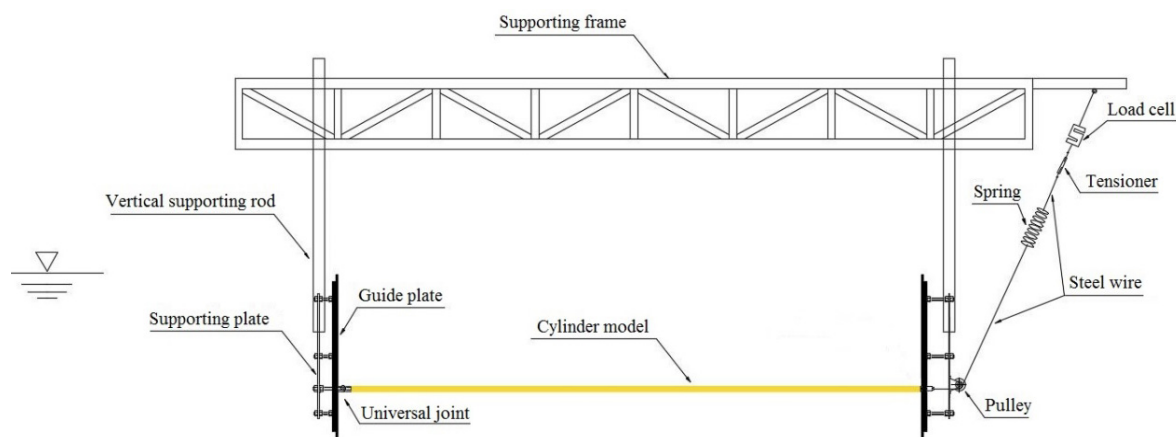


Figure 1. Layout of the experiments.

The supporting frame was composed of a number of vertical and horizontal steel beams. Each vertical supporting unit consisted of a vertical supporting rod, a supporting plate, and a guide plate. The vertical supporting rods were connected to the supporting plates at the bottom end and the supporting frame at the top end, respectively. The guide plate was installed on the inner side of the supporting plate by several long bolts to ensure that the flow around the towing cylinder model was two-dimensional.

The cylinder model was pinned at one end using a universal joint and connected with a steel wire at the other end. The steel wire passed through two small hollow poles (one on the guide plate and the other on the supporting plate) and was connected to a spring at the end. The use of the spring allowed a gradual variation of axial tension on the cylinder model during the experiment. Four axial tensions of 0 N, 50 N, 100 N and 150 N were employed by adjusting the tensioner. A load cell was adopted to monitor the axial tension on the vibrating flexible cylinder. A pulley was used to change the direction of the steel wire. The flexible cylinder model was placed 1.0 m under the still water level, and the free-surface effect was negligible.

As shown in Figure 2, the flexible cylinder model (with an outer diameter of 20 mm and a length of 3.91 m) was made of a coaxial composite tube. The inner tube was a steel pipe with an outer diameter of 19.8 mm and a wall thickness of 2.0 mm. The outer tube was a heat shrinkable PVC pipe with an outer diameter of 20.0 mm and a wall thickness of 0.1 mm. The use of the outer PVC pipe was due to the fact that it could provide a smooth external surface but also protect and insulate the instrumentation cables and strain gauges. The mass per unit length,  $m_s$ , of the cylinder model, including the mass of

the measuring instruments and the trapped water inside the steel pipe, was 0.573 kg/m, resulting in a dimensionless mass ratio ( $m^* = 4m_s/\rho\pi D^2$ , where  $\rho$  is the density of water) of 1.39. The bending stiffness of the cylinder model,  $EI$  (see Table 1), was 324.94 N·m<sup>2</sup>. The structural damping ratio,  $\zeta$  (measured in a free-decaying test of the cylinder model in water), was 0.0598. The axial tension was directly employed on the inner steel pipe. Ten pairs of strain gauges were attached to the outer surface of the steel pipe and covered by the PVC pipe. Five of those were oriented in the  $x$ -direction (streamwise) while the others were in the  $y$ -direction (transverse). The measuring points were evenly distributed along the cylinder model, as illustrated in Figure 3. The aspect ratio (length to diameter) of the cylinder model was 195.5. The key parameters of the cylinder model are listed in Table 1.

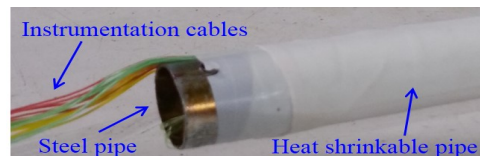


Figure 2. Flexible cylinder model.

Table 1. Key parameters of the cylinder model.

Items	Values
Cylinder model length, $L$	3.91 (m)
Outer diameter, $D$	0.020 (m)
Aspect ratio, $L/D$	195.5
Bending stiffness, $EI$	324.94 (N·m <sup>2</sup> )
Axial tension, $T$	0, 50, 100, 150 (N)
1st order natural frequency in still water, $f_1$	1.96, 2.18, 2.38, 2.56 (Hz)
Mass per unit length (with trapped water), $m_s$	0.573 (kg/m)
Mass ratio, $m^*$	1.39
Structural damping ratio in still water, $\zeta$	0.0598

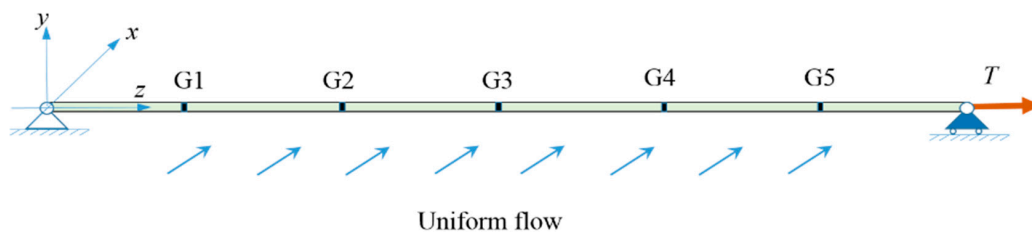


Figure 3. Locations of strain gauges along the cylinder model.

The cylinder model was towed horizontally in still water with a velocity from 0.05 m/s to 0.15 m/s with an increment of 0.05 m/s. The corresponding Reynolds number ranged from 1000 to 3000, approximately. In this paper, we mainly focused on the pure streamwise VIV of the flexible slender cylinder. However, the motion of the cylinder in our experimental tests was not constrained; it could vibrate in the transverse and streamwise directions. The sampling frequency of the measuring instruments was 50 Hz, which was sufficient to avoid aliasing problems. Each experimental run held for 40 s, and the data measured in the last 30 s was used for analysis. A total of 12 runs were carried out.

### 3. Modal Analysis Approach

In order to eliminate the noises from the measured strain signals, a band-pass filtering, ranging from 0.5 to 30 Hz, was applied. Next, the filtered data was used in the modal analysis to obtain the displacement responses of the cylinder model. Assuming that the time-varying displacement could be expressed as a sum of the product of the mode shapes and the modal weights:

$$x(z, t) = \sum_{n=1}^{\infty} w_n(t) \varphi_n(z) \quad (1)$$

where  $x(z, t)$  is the time varying displacement in the streamwise direction,  $z$  is the coordinate along the axis of the cylinder model,  $t$  is time,  $w_n(t)$  is the modal weight,  $\varphi_n(z)$  is the mode shape, and  $n = 1, 2, 3, \dots$  is the order of vibration mode.

For the pinned–pinned boundary conditions applied in the present experiment, the  $n$ th mode shape could be written as:

$$\varphi_n(z) = \sin \frac{n\pi z}{L} \quad (2)$$

where  $L$  is the length of the cylinder model. Taking into account the relationship between curvature and strain (i.e.,  $k(z, t) = \varepsilon(z, t)/R$ ), Equation (2) resulted in:

$$\frac{\varepsilon(z, t)}{R} = k(z, t) = x''(z, t) = -\sum_{n=1}^{\infty} \left(\frac{n\pi}{L}\right)^2 w_n(t) \sin \frac{n\pi z}{L} \quad (3)$$

where  $R$  denotes the radius of the cylinder model. In Equation (3), the unknown time-varying modal weight  $w_n(t)$  could be calculated using the filtered strain signals. Readers are referred to Chaplin et al. [29], Trim et al. [30], Lie and Kaasen [31], and Song et al. [32] for more details about the modal analysis approach.

Figure 4 shows an example of the modal analysis. The left column plots gave the time histories of the strain signals measured at five measuring points during the last 30 s. The corresponding modal weights evaluated using Equation (3) are depicted in the middle column plots. It can be seen that the streamwise displacement response was dominated by the first mode in this case. The time histories of the displacement at the five measuring points were calculated using Equation (1), and are presented in the right column plots. In the following section, the displacement responses were obtained by the modal analysis approach, which was introduced in this section.

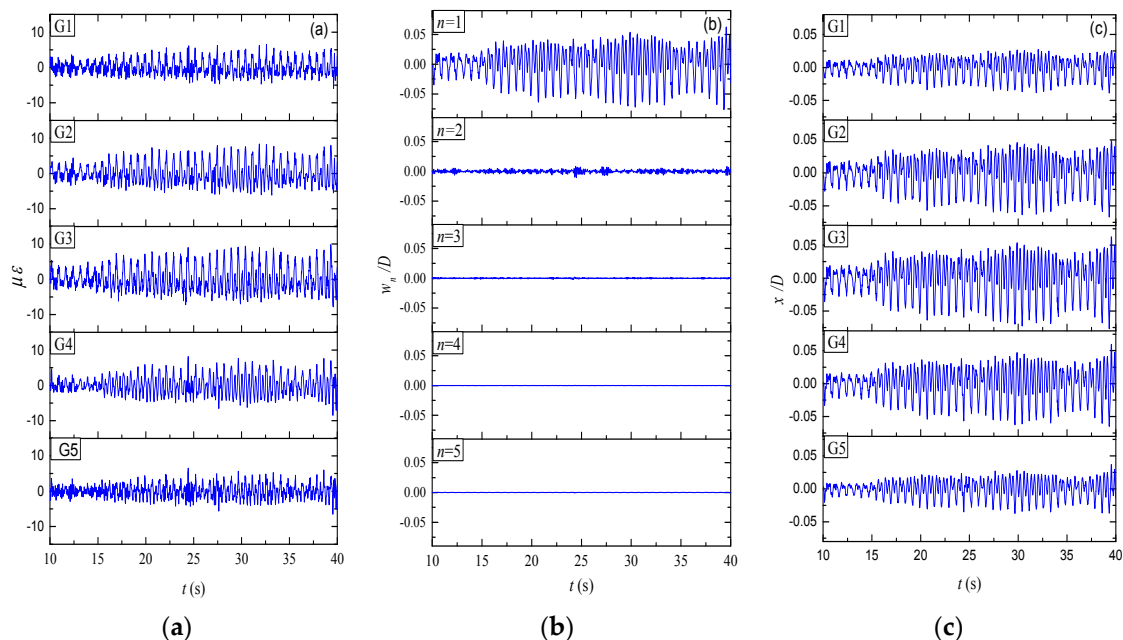


**Figure 4.** An example of the modal analysis approach with the axial tension ( $T = 150$  N) and towing velocity ( $u = 0.15$  m/s). (a) Streamwise strain signals at five measuring points; (b) modal weights of streamwise VIV; and (c), time histories of the displacements at five measuring points.



#### 4. Results and Discussion

Figure 5 shows the root-mean-square (RMS) values of the normalized streamwise response amplitude  $x_{RMS}/D$  versus the reduced velocity  $V_r$ . Clearly, there are two response branches separated by a low-amplitude region at  $V_r \approx 1/(2S_t)$ , where  $S_t$  is the Strouhal representing the vortex-shedding frequency of flow past a stationary cylinder. In the present results, the first excitation region is  $1.0 < V_r < 2.6$ , while the second one is  $2.6 < V_r < 4.0$ . The peak value of the normalized RMS amplitude in the first excitation region is roughly 0.07, which is slightly smaller than its counterpart of 0.08 in the second excitation region. The experimental results of Okajima et al. [20] and Cagney and Balabani [23] on the streamwise VIV of a rigid cylinder elastically-mounted on both ends (2D), and a cantilevered flexible cylinder (3D) in a water tunnel, were superimposed in Figure 5. The present results agree well with those of Cagney and Balabani [23] and the 3-D results of Okajima et al. [20], but deviate from the 2D results of Okajima et al. [20]. This can be attributed to the different reduced mass-damping parameters adopted in these studies. In the present study,  $C_n = 0.167$ , which is similar to that of 0.083 in Cagney and Balabani [23], and 0.24 in the 3D tests of Okajima et al. [20], but significantly smaller than 0.98 in the 2D tests of Okajima et al. [20]. However, in the second excitation region, the present results show a broader range than those in Okajima et al. [20] and Cagney and Balabani [23]. The peak value is comparable to the 3D results of Okajima et al. [20], but obviously larger than those in Cagney and Balabani [23], and the 2D tests of Okajima et al. [20]. A possible reason is the flexible slender cylinder with a very large aspect ratio adopted in this study. It is worth noting that the results presented in Figure 5 are actually a combination of the results with four different axial tensions. As mentioned above, the towing velocity of the carriage in the experiments is from 0.05 m/s to 0.15 m/s, with an increment of 0.05 m/s, restricted by the minimum resolution of the towing tank facility. A total of three reduced velocities were investigated for a given axial tension, which is far from enough to properly depict the variation of response amplitude. However, by carefully selecting the axial tensions and combining the results with different axial tensions, more data points can be reasonably distributed in the range of  $1.0 < V_r < 4.0$ , due to different  $f_1$  adopted in the normalization of the reduced velocity. In general, the reasonable agreement between different results provides strong evidence of the reliability of the experimental set-up and the validity of the post-processing approaches for the measurement data.

At the transition region, i.e.,  $V_r \approx 2.5$ , between two excitation branches, the streamwise vibration amplitude showed quite a large variation between different experiments. The minimum RMS amplitude was nearly zero in the 2D results of Okajima et al. [20], while the maximum value could be as high as  $x_{RMS}/D \approx 0.06$  in the 3D results of Okajima et al. [20]. The authors attributed it to the aspect ratio (AR) effects, i.e., the manner in which the depth of the valley between the first and second excitation region decreases with decreasing AR. When the  $AR < 10$ , only a single excitation region was found in the cantilevered cylinder tests of Okajima et al. [20]. Nakamura et al. [33] concluded from their cantilevered cylinder experiments that the streamwise amplitude did not show a significant reduction in the transition region, when  $AR < 21$  and this trend became even more prevailing with decreasing AR. The results of this study, i.e.,  $x_{RMS}/D \approx 0.01$  with  $AR = 195.5$ , provide supporting data for the conclusion.

Figure 6 presents the dimensionless streamwise and transverse maximum amplitudes versus the reduced velocity, together with the normalized frequencies in both directions. It can be seen that the transverse amplitude was much smaller than its streamwise counterpart in the first excitation region. The peak values,  $x_{Max}/D \approx 0.12$  (streamwise) and  $y_{Max}/D \approx 0.03$  (transverse), were simultaneously obtained at  $V_r \approx 2.3$ . The non-dimensional vibration frequencies, normalized by the first order natural frequencies of the cylinder model under different axial tensions, were roughly unified in the first excitation region (i.e.,  $f_x \approx f_y \approx f_1$ , where  $f_x$  and  $f_y$  were the dominant response frequencies in the streamwise and transverse directions, respectively). This agrees with the results of Blevins and Coughran [34], in which a 2-DOF spring-supported rigid cylinder was tested.

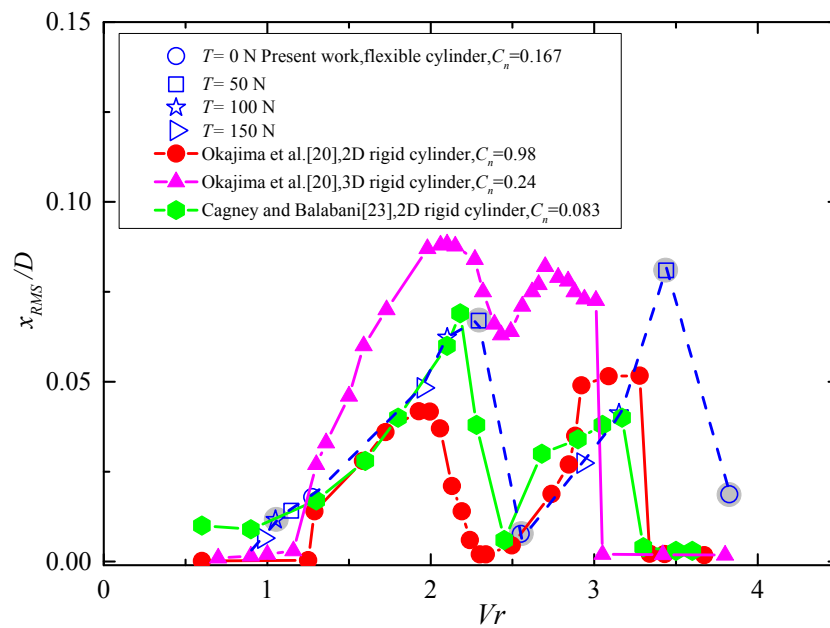


**Figure 5.** Dimensionless streamwise root-mean-square (RMS) response amplitudes versus the reduced velocity (grey circles represent five typical streamwise VIV response regions, which will be discussed later, including the beginning of the first excitation region, the maximum streamwise amplitude in the first excitation region, the transition region between the first and second excitation region, the maximum streamwise amplitude in the second excitation region, and the end of the second excitation region).

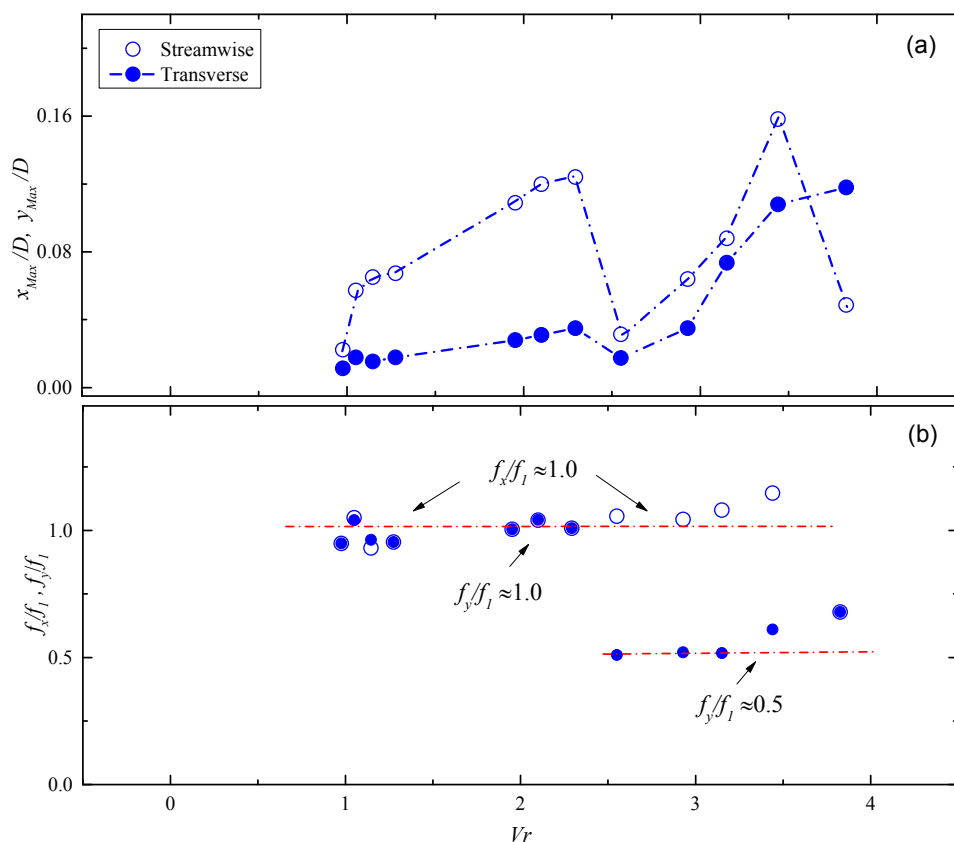


**Figure 6.** Dimensionless maximum amplitudes: (a) in the streamwise and transverse directions, together with the frequency ratios, and (b), versus the reduced velocity.

Figure 7 shows the  $x$ - $y$  trajectories of the cylinder at  $V_r \approx 2.3$ , together with the distribution of  $x_{RMS}/D$  along the axis of the cylinder model. In the first excitation region, the cylinder followed a slightly inclined linear orbit, which agrees with the results in the 2D tests (elastically-supported rigid cylinder) of Jauvtis and Williamson [9] and Blevins and Coughran [34], but is different from the flat figure-of-eight trajectory observed in the 3D tests (pivoted cylinder) of Cagney and Balabani [7]. At the transition point of  $V_r \approx 2.6$ , the ratio between the streamwise and transverse frequencies was roughly 2, i.e.,  $f_x \approx 2f_y \approx f_1$ , due to the alternate vortex shedding, which indicates the onset of the “lock-in” phenomenon and the beginning of the monotonic increase of the transverse amplitude. In the second excitation, the frequency ratio was kept at  $f_x \approx 2f_y$  and the orbit of the cylinder showed a figure-of-eight pattern, as shown in Figure 8. These observations are consistent with those in Jauvtis and Williamson [9], Blevins and Coughran [34], and Cagney and Balabani [7], except that the figure-of-eight was slightly skewed at the top side. At the end of the second excitation region,  $V_r \approx 3.8$ , a significant drop could be found in  $f_x/f_1$  and the vibration frequencies in the streamwise and transverse directions became equal again. The streamwise vibration frequency obviously fell outside the resonance region, which resulted in the large reduction in the streamwise maximum amplitude. The transverse maximum amplitude shows a mild increment at this reduced velocity, which agrees with the results of Jauvtis and Williamson [9], but disagrees with those in Cagney and Balabani [7], where the transverse maximum amplitude plummeted.

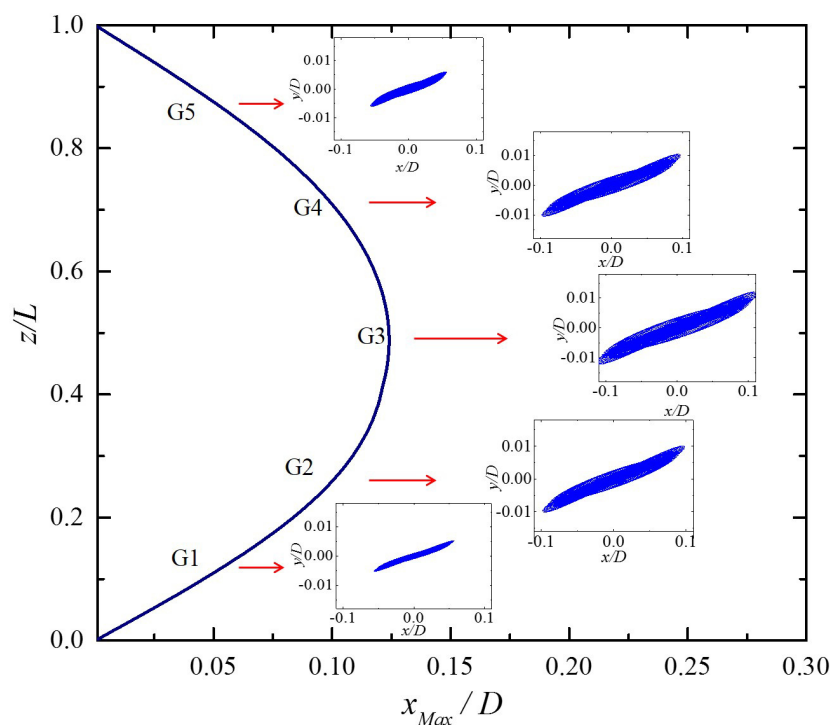


Figure 7.  $x$ - $y$  trajectories of the cylinder in the first excitation region with  $V_r \approx 2.3$ .

The typical streamwise VIV behaviors of a flexible cylinder were further investigated in the following part. Five representative cases, as indicated by the markers with grey shadow in Figure 5, were selected. These representative cases corresponded to the initial zone, middle of the first excitation region, the transition region, and the middle and end of the second excitation region, respectively.

Figures 9–13 give the streamwise displacement response and vibration frequency spectra at five measuring points. The first column graph shows the time history of streamwise displacement for the last 30 s of a complete sampling period at different measuring positions along the cylinder model. The second column graph presents the time history in a short time interval, from 28 s to 30 s, in order to clearly describe the characteristics of oscillation. The third column graph illustrates the



displacement response spectra, which was produced by fast Fourier transformation (FFT) analysis of the displacement data.

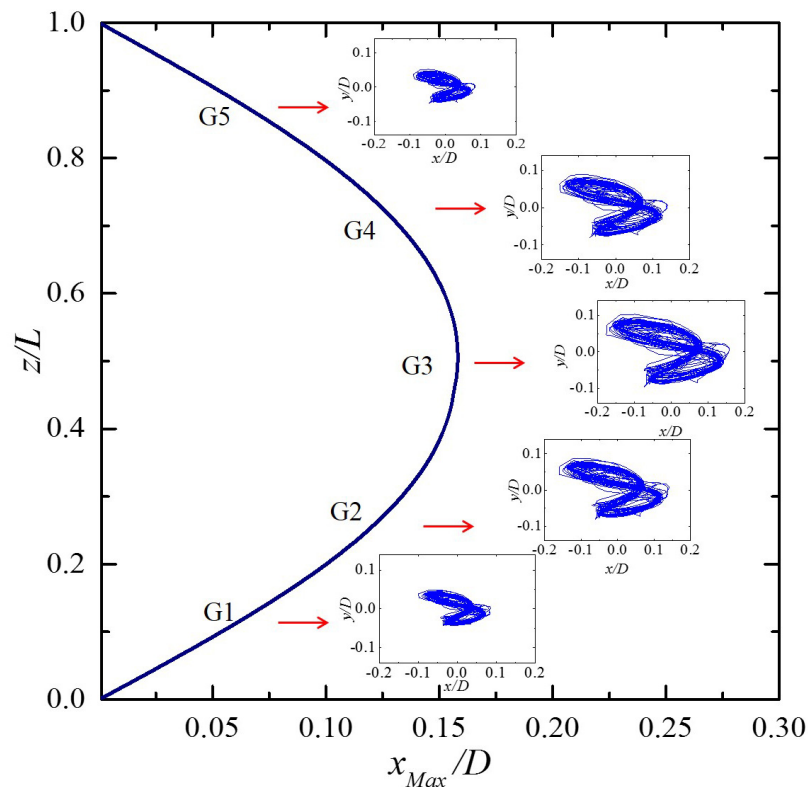


**Figure 8.**  $x$ - $y$  trajectories of the cylinder in the second excitation region, with  $V_r \approx 3.4$ .

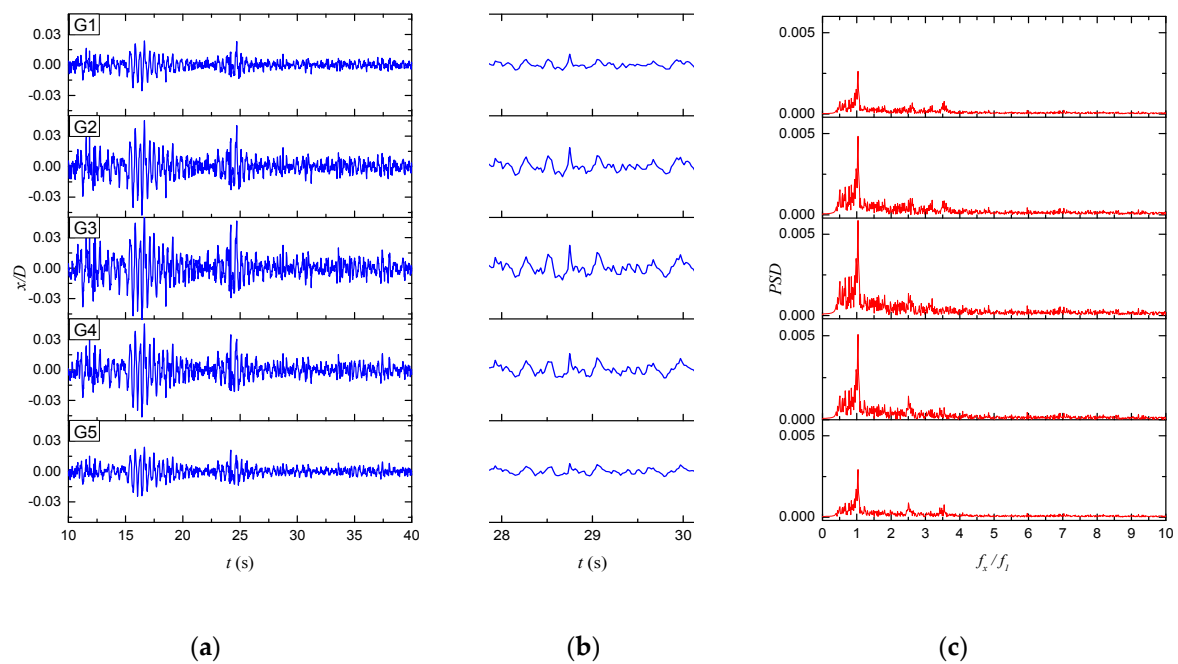


**Figure 9.** Time histories and spectral plots of streamwise displacement with  $V_r \approx 1.05$ . (a) Time-varying streamwise displacement for the last 30 s of a complete sampling period at five measuring positions along the cylinder model; (b) time history of streamwise displacement in a short time interval, from 28 s to 30 s; and (c) displacement response spectra.

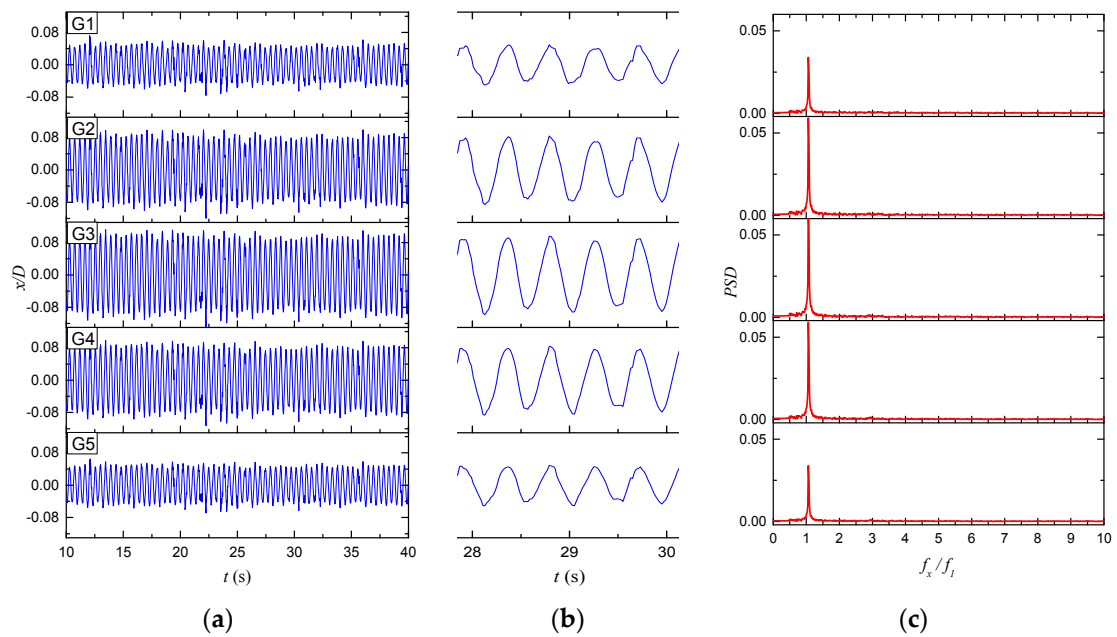


**Figure 10.** Time histories and spectral plots of streamwise displacement with  $V_r \approx 2.29$ . (a) Time-varying streamwise displacement for the last 30 s of a complete sampling period at five measuring positions along the cylinder model; (b) time history of streamwise displacement in a short time interval, from 28 s to 30 s; and (c) displacement response spectra.

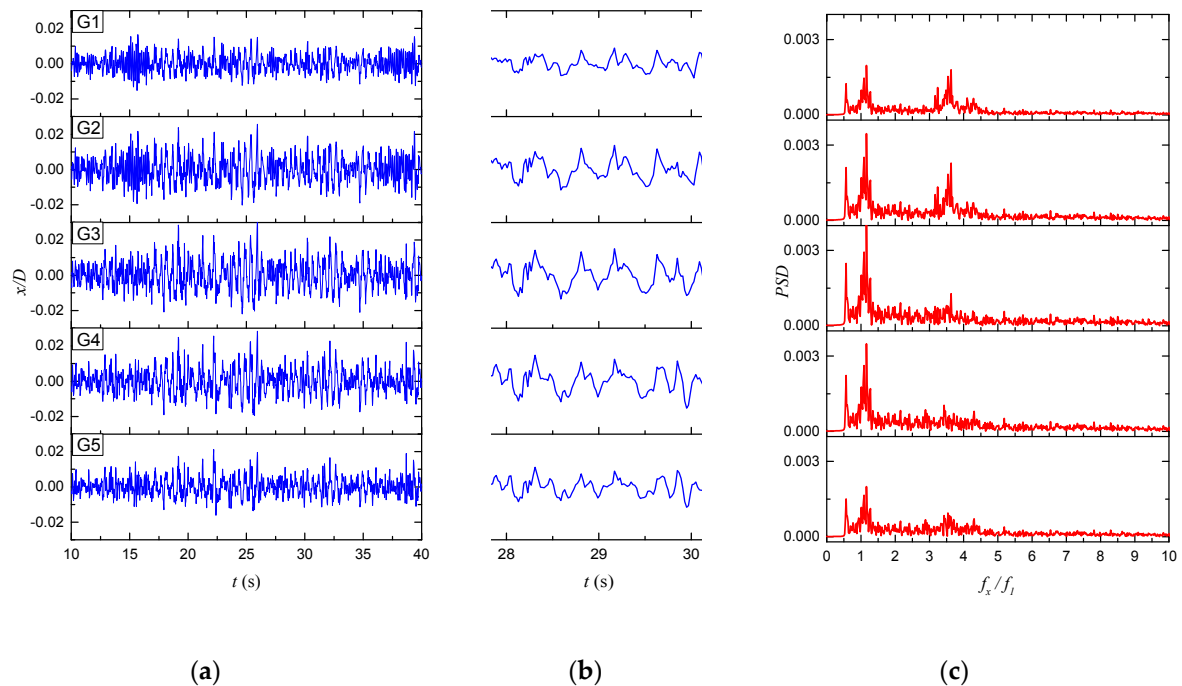


**Figure 11.** Time histories and spectral plots of streamwise displacement with  $V_r \approx 2.55$ . (a) Time-varying streamwise displacement for the last 30 s of a complete sampling period at five measuring positions along the cylinder model; (b) time history of streamwise displacement in a short time interval, from 28 s to 30 s; and (c) displacement response spectra.

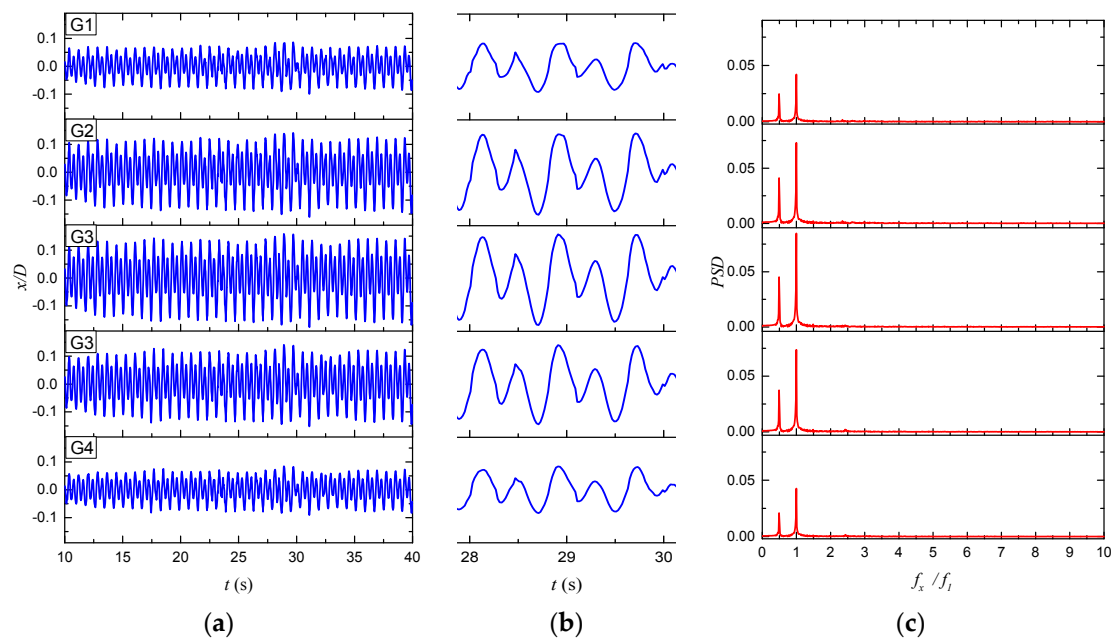


**Figure 12.** Time histories and spectral plots of streamwise displacement with  $V_r \approx 3.44$ . (a) Time-varying streamwise displacement for the last 30 s of a complete sampling period at five measuring positions along the cylinder model; (b) time history of streamwise displacement in a short time interval, from 28 s to 30 s; and (c) displacement response spectra.

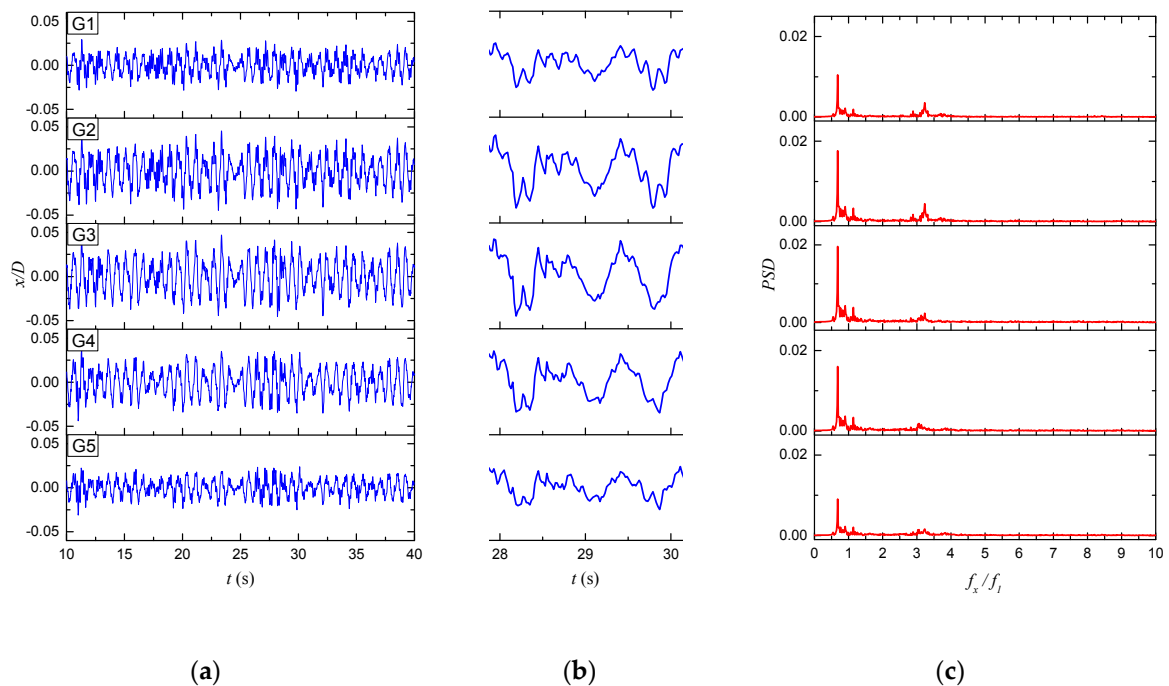


**Figure 13.** Time histories and spectral plots of streamwise displacement with  $V_r \approx 3.83$ . (a) Time-varying streamwise displacement for the last 30 s of a complete sampling period at five measuring positions along the cylinder model; (b) time history of streamwise displacement in a short time interval, from 28 s to 30 s; and (c) displacement response spectra.

At the beginning of the first excitation region, the time history of the streamwise displacement, characterized by a small amplitude, was irregular and aperiodic, as shown in Figure 9. A similar

phenomenon was also observed in the rigid cylinder experiments of Cagney and Balabani [22] and was attributed to the turbulent buffeting effects. The vibration amplitude of the flexible cylinder at the mid-span was generally larger than those near the pinned-ends due to the predominant first mode of vibration. The spectral plot showed a large peak at the frequency ratio of  $f_x/f_1 \approx 1.0$  and numerous small spikes, indicating some unsteadiness in the vortex shedding.

When the streamwise amplitude peaked in the first excitation region, the time history of the streamwise displacement showed a quasi-sinusoidal curve, except small irregularities observed at the measuring points near the pinned-ends of the cylinder model, as shown in Figure 10. In addition, it could be found that the dimensionless maximum displacement amplitude was roughly equal to 0.12, which was larger than the rigid cylinder results of Cagney and Balabani [22], where the dimensionless maximum displacement amplitude was between 0.06 and 0.09, with minor fluctuations in the middle of the first response branch. The spectral plot for the streamwise displacement was rather pure, with only one predominant peak observed at  $f_x/f_1 \approx 1.0$ .

In the second excitation region, the streamwise displacement showed evident beatings in its time history, as shown in Figure 12. The time history of the displacement response was regular and periodic, and attained the maximum amplitude of 0.16. Two large peaks were found in the spectral plot. One occurred at  $f_x/f_1 = 1.0$ , and the other occurred at one-half of this value, which was apparently the effects of the transverse vibrations. Blevins and Coughran [34] performed the laboratory tests on the vortex-induced vibration of an elastically supported cylinder, which could vibrate in streamwise and transverse directions, and could also be constrained to move only in a streamwise direction. In the first branch, they found that the transverse response could be negligible, while the freedom to move in the transverse directions had a significant effect on streamwise VIV in the second branch. The frequency of the transverse oscillations was equal to half the frequency of the streamwise vibrations, and the cylinder followed a figure-of-eight trajectory in the second branch [7]. This is the reason why two frequency peaks can be seen in the plot of spectra of the displacement in Figure 12.

At the end of the second excitation region, irregularities were checked one more time in the time history of the streamwise displacement, as shown in Figure 13. However, different from the results shown in Figures 9 and 11, a predominant peak which obviously deviated from  $f_x/f_1 \approx 1.0$  was observed in the spectral plot, indicating the end of the resonance.

Previous experiments carried out during the past several decades indicate that the maximum amplitude of a transverse VIV is highly dependant on a combined mass-damping parameter  $m^*\zeta$ . The so-called ‘Griffin plot’ is presented by compiling a large variety of investigations on VIV [3,5]. Although there are conflicting opinions regarding its validity, the Griffin plot is widely used in industry and academic fields. Similarly, it was also proved that the maximum amplitude of the streamwise VIV followed closely with the reduced mass-damping parameter  $C_n$  [20,24,34,35]. A series of experiments on streamwise VIV of a circular cylinder was carried out by Okajima and colleagues [20,33,36,37] to investigate the sensitivity of the amplitude response to  $C_n$ . In this study, an extensive compilation of a large variety of published data, together with the present results, is depicted in two log–log plots, as shown in Figure 14. Two least-square fitted curves are superimposed on the plots and their expressions are defined as:

$$x_{1st\_Max}/D = 0.131e^{-1.01C_n} \quad (4)$$

in the first excitation region (see Figure 14a); and

$$x_{2nd\_Max}/D = 0.135e^{-0.663C_n} \quad (5)$$

in the second excitation region (see Figure 14b). It is shown that the two curves follow closely with the data, especially when  $C_n < 1.0$ , which covers the majority of the streamwise VIV of marine cylinders. A small deviation can be observed at a larger  $C_n$ . These two formulae could be used to predict the response amplitudes according to the mass-damping parameter  $C_n$ .

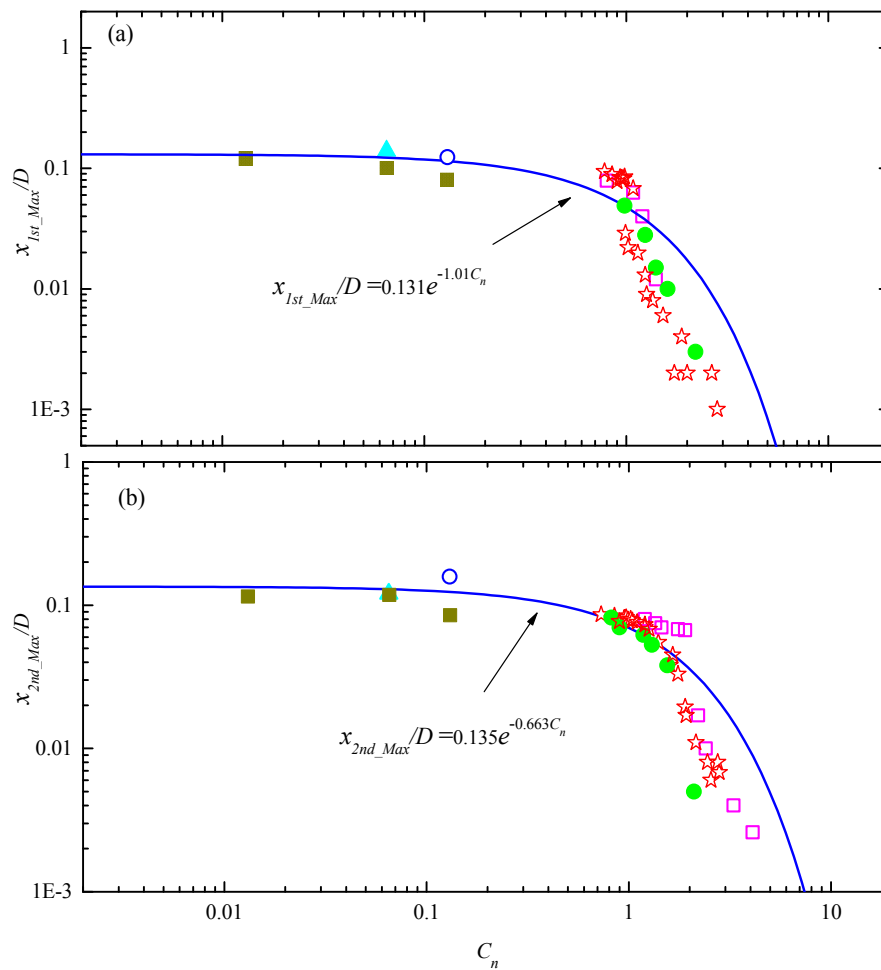


**Figure 14.** Maximum dimensionless streamwise displacements versus mass-damping parameters in the first (a) and second excitation regions (b). (■ Blevins and Coughran [34], water; ▲ Jauvtis and Williamson [9], water; □ Matsuda et al. [35], air; ● Okajima et al. [20], water; ☆ Okajima et al. [20], air; ○ present experimental data; — fitted curve).

## 5. Conclusions

Laboratory experiments on streamwise VIV of a flexible slender cylinder were performed in the towing tank facility at Tianjin University. The cylinder model was made of a coaxial composite tube with a length of 3.91 m and an outer diameter of 20.0 mm, resulting in a large aspect ratio of 195.5. The mass ratio of the cylinder model was 1.39 and the structural damping ratio was 0.0598. Strain gauges were used to measure structural strain responses at five points evenly distributed along the cylinder. The modal analysis method was applied to transform the measured strain signals to the response displacement.

It was found that the RMS amplitudes in the streamwise direction reasonably agreed with the published data, which verified the fidelity of the experimental set-up and the post-processing approaches. For the streamwise VIV with 3D characteristics, the vibration amplitude in the transition region decreased with the increasing aspect ratio, and the present results provided supporting data for the conclusion. In the first excitation region, compared to the transverse response, the streamwise response showed an equivalent dominant vibration frequency but a much larger amplitude, resulting in a slightly inclined linear orbit in the  $x$ - $y$  plane. However, in the second excitation region, the streamwise frequency was twice that in the transverse direction, and skewed figure-of-eight trajectories were observed. A pure spectral plot and a quasi-sinusoidal time history were observed when the vibration amplitude was large. A broad-peak spectral plot and an irregular and aperiodic time history were

detected when the vibration amplitude was small. Finally, two least-square fitted curves were presented by compiling a large variety of investigations on streamwise VIV.

**Acknowledgments:** The authors would like to acknowledge the financial support of National Natural Science Foundation of China (Grants Nos. 51479135, 51679167 and 51579175), the Science Fund for Creative Research Groups of the National Natural Science Foundation of China (Grant no. 51621092).

**Author Contributions:** Wenqi Qin and Wanhai Xu carried out the experimental tests; Xifeng Gao analyzed the experimental data; Wanhai Xu wrote the paper.

**Conflicts of Interest:** The authors declare no conflict of interest.

## References

1. Naudascher, E. Flow-induced streamwise vibrations of structures. *J. Fluids Struct.* **1987**, *1*, 265–298. [[CrossRef](#)]
2. Norberg, C. Fluctuating lift on a circular cylinder: Review and new measurements. *J. Fluids Struct.* **2003**, *17*, 57–96. [[CrossRef](#)]
3. Sarpkaya, T. A critical review of the intrinsic nature of vortex induced vibrations. *J. Fluids Struct.* **2004**, *19*, 389–447. [[CrossRef](#)]
4. Gabbai, R.D.; Benaroya, H. An overview of modeling and experiments of vortex-induced vibration of circular cylinders. *J. Sound Vib.* **2005**, *282*, 575–616. [[CrossRef](#)]
5. Williamson, C.H.K.; Govardhan, R. A brief review of recent results in vortex-induced vibrations. *J. Wind Eng. Ind. Aerodyn.* **2008**, *96*, 713–735. [[CrossRef](#)]
6. Wu, X.; Ge, F.; Hong, Y. A review of recent studies on vortex-induced vibrations of long slender cylinders. *J. Fluids Struct.* **2012**, *28*, 292–308. [[CrossRef](#)]
7. Cagney, N.; Balabani, S. Streamwise vortex-induced vibrations of cylinders with one and two degrees of freedom. *J. Fluid Mech.* **2014**, *758*, 702–727. [[CrossRef](#)]
8. Feng, Z.; Naibin, J.; Fenggang, Z.; Yixiong, Z.; Xuan, H.; Wanjun, W. Nonlinear characteristics analysis of vortex-induced vibration for a three-dimensional flexible tube. *Commun. Nonlinear Sci. Numer. Simul.* **2016**, *34*, 1–11. [[CrossRef](#)]
9. Jauvtis, N.; Williamson, C.H.K. Vortex-induced vibration of a cylinder with two degrees of freedom. *J. Fluids Struct.* **2003**, *17*, 1035–1042. [[CrossRef](#)]
10. Zhao, M.; Cheng, L.; An, H.; Lu, L. Three-dimensional numerical simulation of vortex-induced vibration of an elastically mounted rigid circular cylinder in steady current. *J. Fluids Struct.* **2014**, *50*, 292–311. [[CrossRef](#)]
11. Wanderley, J.B.V.; Soares, L.F.N. Vortex-induced vibration on a two-dimensional circular cylinder with low Reynolds number and low mass-damping parameter. *Ocean Eng.* **2015**, *97*, 156–164. [[CrossRef](#)]
12. Govardhan, R.; Williamson, C.H.K. Modes of vortex formation and frequency response of a freely vibrating cylinder. *J. Fluid Mech.* **2000**, *420*, 85–130. [[CrossRef](#)]
13. Bearman, P.W. Circular cylinder wakes and vortex-induced vibrations. *J. Fluids Struct.* **2011**, *27*, 648–658. [[CrossRef](#)]
14. Raghavan, K.; Bernitsas, M.M. Experimental investigation of Reynolds number effect on vortex induced vibration of rigid circular cylinder on elastic supports. *Ocean Eng.* **2011**, *38*, 719–731. [[CrossRef](#)]
15. Griffin, O.M.; Ramberg, S.E. Vortex shedding from a cylinder vibrating in line with an incident uniform flow. *J. Fluid Mech.* **1976**, *75*, 257–271. [[CrossRef](#)]
16. Baarholm, G.S.; Larsen, C.M.; Lie, H. On fatigue damage accumulation from in-line and cross-flow vortex-induced vibrations on risers. *J. Fluids Struct.* **2006**, *22*, 109–127. [[CrossRef](#)]
17. Aguirre, J.E. Flow Induced, In-line Vibrations of a Circular Cylinder. Ph.D. Thesis, Imperial College of Science and Technology, London, UK, 1978.
18. Currie, I.G.; Turnbull, D.H. Streamwise oscillations of cylinders near the critical Reynolds number. *J. Fluids Struct.* **1987**, *1*, 185–196. [[CrossRef](#)]
19. Sumer, B.; Fredsøe, J. *Hydrodynamic around Cylindrical Structures*; World Scientific: Singapore, 1997; p. 69.
20. Okajima, A.; Nakamura, A.; Kosugi, T.; Uchida, H.; Tamaki, R. Flow-induced in-line oscillation of a circular cylinder. *Eur. J. Mech. B. Fluids* **2004**, *23*, 115–125. [[CrossRef](#)]
21. Nishihara, T.; Kanekob, S.; Watanabe, T. Characteristics of fluid dynamic forces acting on a circular cylinder oscillated in the streamwise direction and its wake patterns. *J. Fluids Struct.* **2005**, *20*, 505–518. [[CrossRef](#)]



22. Cagney, N.; Balabani, S. Wake modes of a cylinder undergoing free streamwise vortex-induced vibrations. *J. Fluids Struct.* **2013**, *38*, 127–145. [[CrossRef](#)]
23. Cagney, N.; Balabani, S. Mode competition in streamwise-only vortex induced vibrations. *J. Fluids Struct.* **2013**, *41*, 156–165. [[CrossRef](#)]
24. King, R.; Prosser, M.J.; Johns, D.J. On vortex excitation of model piles in water. *J. Sound Vib.* **1973**, *29*, 169–188. [[CrossRef](#)]
25. Reid, D.L. A model for the prediction of in-line vortex induced vibrations of cylindrical elements in a non-uniform steady flow. *Ocean Eng.* **1991**, *18*, 147–165. [[CrossRef](#)]
26. Sidarta, D.E.; Lambrakos, K.F.; Thompson, H.M.; Burke, R.W. A methodology for in-line VIV analysis of risers in sheared currents. In Proceedings of the 25th International Conference on Offshore Mechanics and Arctic Engineering, OMAE2006-92431, Hamburg, Germany, 4–9 June 2006.
27. Larsen, C.M.; Yttervik, R.; Aronsen, K.H. Calculation of inline vortex induced vibrations of free spanning pipelines. In Proceedings of the 26th International Conference on Offshore Mechanics and Arctic Engineering, OMAE2007-29533, San Diego, CA, USA, 10–15 June 2007.
28. Xu, W.; Gao, X.; Du, J. The prediction on in-line vortex-induced vibration of slender marine structures. *Acta Mech. Sin.* **2012**, *28*, 1303–1308. [[CrossRef](#)]
29. Chaplin, J.R.; Bearman, P.W.; Huera-Huarte, F.J.; Pattenden, R.J. Laboratory measurements of vortex-induced vibrations of a vertical tension riser in a stepped current. *J. Fluids Struct.* **2005**, *21*, 3–24. [[CrossRef](#)]
30. Trim, A.D.; Braaten, H.; Lie, H.; Tognarelli, M.A. Experimental investigation of vortex-induced vibration of long marine risers. *J. Fluids Struct.* **2005**, *21*, 335–361. [[CrossRef](#)]
31. Lie, H.; Kaasen, K.E. Modal analysis of measurements from a large-scale VIV model test of a riser in linearly sheared flow. *J. Fluids Struct.* **2006**, *22*, 557–575. [[CrossRef](#)]
32. Song, J.; Lu, L.; Teng, B.; Park, H.; Tang, G.; Wu, H. Laboratory tests of vortex-induced vibrations of a long flexible riser pipe subjected to uniform flow. *Ocean Eng.* **2011**, *38*, 1308–1322. [[CrossRef](#)]
33. Nakamura, A.; Okajima, A.; Kosugi, T. Experiments on flow-induced in-line oscillation of a circular cylinder in a water tunnel (2<sup>nd</sup> report, influence of the aspect ratio of a cantilevered circular cylinder). *JSME Int. J. Ser. B* **2001**, *44*, 705–711. [[CrossRef](#)]
34. Blevins, R.D.; Coughran, C.S. Experimental investigation of vortex-induced vibration in one and two dimensions with variable mass, damping, and Reynolds number. *J. Fluids Eng.* **2009**, *131*, 101202. [[CrossRef](#)]
35. Matsuda, K.; Uejima, H.; Sugimoto, T. Wind tunnel tests on in-line oscillation of a two-dimensional circular cylinder. *J. Wind Eng. Ind. Aerodyn.* **2003**, *91*, 83–90. [[CrossRef](#)]
36. Okajima, A.; Kosugi, T.; Nakamura, A. Experiments on flow-induced in-line oscillation of a circular cylinder in a water tunnel (1st report, the difference of the response characteristics when a cylinder is elastically supported at both ends and cantilevered). *JSME Int. J. Ser. B* **2001**, *44*, 695–704. [[CrossRef](#)]
37. Okajima, A.; Kosugi, T.; Nakamura, A. Flow-induced in-line oscillation of a circular cylinder in a water tunnel. *J. Pressure Vessel Technol.* **2002**, *124*, 89–96. [[CrossRef](#)]

